ULTRAVIOLET THROUGH NEAR-INFRARED REFLECTANCE VARIATION ON MERCURY AND THE SEARCH FOR MINERALOGICAL TELLTALES. Noam R. Izenberg (noam.izenberg@jhuapl.edu)[1], Gregory M. Holsclaw[2], Deborah L. Domingue[3], William E. McClintock[2], Rachel L. Klima[1], David T. Blewett[1], Mark C. Kochte[1], Jörn Helbert[4], Mario D'Amore[4], Ann L. Sprague[5], Faith Vilas[3], and Sean C. Solomon[6]. [1]The Johns Hopkins University Applied Physics Laboratory, Laurel, MD 20723, USA; [2]Laboratory for Atmospheric and Space Physics, University of Colorado, Boulder, CO 80303, USA; [3]Planetary Science Institute, Tucson, AZ 85719, USA; [4]DLR, Rutherfordstrasse 2, Berlin, Germany; [5]Lunar and Planetary Laboratory, University of Arizona, Tucson, AZ 85721, USA; [6]Department of Terrestrial Magnetism, Carnegie Institution of Washington, Washington, DC 20015, USA.

Introduction: The MESSENGER spacecraft's [1] Mercury Atmospheric and Surface Composition Spectrometer (MASCS) [2] has been mapping the planet's surface and exosphere from orbit since 29 March 2011 and has obtained more than 1.3 million near-ultraviolet to near-infrared spectra of Mercury's surface during the first nine months of operations. The Visible and Infrared Spectrograph (VIRS) channel on MASCS covers the wavelength range 300-1450 nm. VIRS reflectance spectra have so far shown no clear evidence of the absorption band centered near a wavelength of 1 μm (1000 nm) associated with the presence of ferrous iron in silicates. The lack of this absorption and evidence of ultraviolet (UV) absorption showrtward of 300 nm is consistent with the possibility of very low iron content (2-4 wt% FeO) [3].

VIRS Mapping Measurements: Systematic VIRS mapping of Mercury has sampled all geologic regions of the planet. Fig. 1 is a red-green-blue (RGB) composite of VIRS spectral information overlaid on a Mercury Dual Imaging System (MDIS) [4] base map. The R channel is MASCS VIRS reflectance at 575 nm, a proxy for visible (VIS) albedo; the G channel is the 415-nm/750-nm reflectance ratio, a proxy for visible-near infrared (VIS-NIR) spectral slope; and the B channel is the 310-nm/390-nm reflectance ratio, indicating the relative strength of UV absorption features. The map is limited to observations at less than 70° incidence angle and less than 35° C detector temperature. Spectra have had a preliminary empirical photometric correction applied.

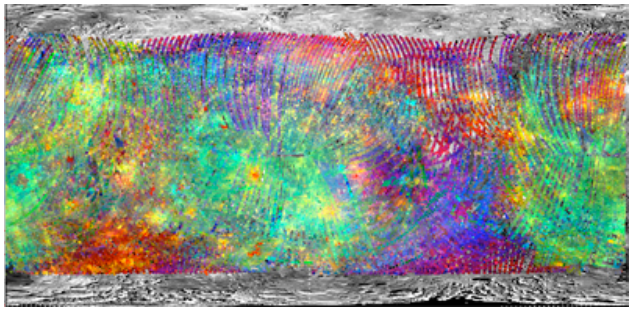

Fig. 1. Composite MASCS VIRS global coverage map overlaid on MDIS monochrome mosaic. Over 700,000 individual MASCS footprints are represented in colors indicating spectral properties (refer to text for color assignments).

The global composite map reveals regional spectral variations due to all three parameters. We examine individual locations and unit types in more detail to begin to interpret the origin of these variations.

UV-NIR Differences and Geologic Units: We investigate a subset of four geologic units, earlier defined [5-7], differentiable by contrasts in UV through NIR spectral properties. These units, low-reflectance material (LRM), pyroclastic material, hollows, and fresh craters, represent possible "end members," distinct in spectral properties and geology. MDIS images of each example appear morphologically uniform within the sampling VIRS footprint and therefore should be relatively free of mixing with other materials. Spectra of several examples of the four different units are shown in Figs. 2 and 3. In addition to examining spectra directly, we ratio spectra from each locality to a "mean Mercury" spectrum, allowing slope differences to be more clearly characterized.

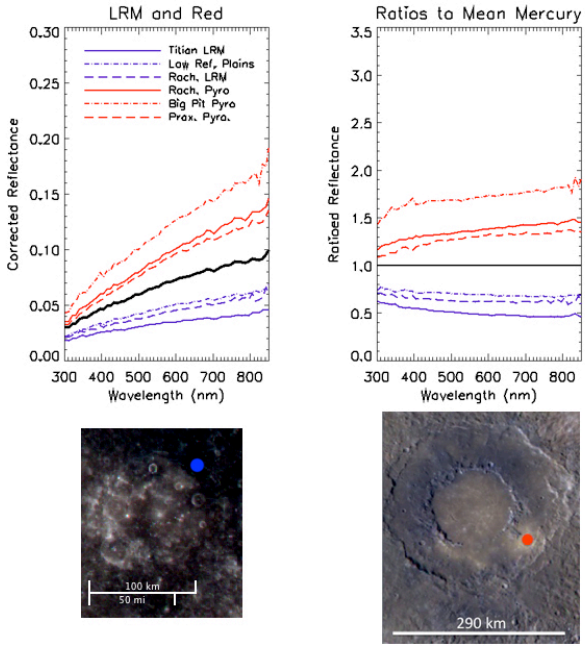

Fig. 2. LRM and pyroclastic material shown as VIRS reflectance spectra from 300 to 895 nm; LRM in blue, pyroclastics in red. Left plot is reflectance; right is ratio to Mercury mean. Images show example locations of spectral samples in MDIS color composite (R=1000 nm, G=750 nm, B=430 nm). Left: Titian crater (LRM), Right: Rachmaninoff basin (pyroclastics). Colored dots show locations of selected MASCS footprint in each unit.

All Mercury spectra have the characteristic of increasing reflectance with increasing wavelength, or "red spectral slope." Plots of spectra for LRM and pyroclastic material ratioed to mean Mercury (black lines in Figs. 2 and 3) show that LRM materials are not only darker than mean Mercury but relatively less red sloped, or "bluer." The ratio plots show that pyroclastic materials have steeper UV-VIS slopes than mean Mercury, whereas most LRM materials have shallower slopes in the UV.

Example spectra of hollows and a small, bright, fresh-appearing crater are shown in Fig. 3. The five hollows sampled, although morphologically similar [7], appear to have distinct spectral differences in the UV-VIS. Specifically, hollows materials

plotted in cyan in Fig. 3, typified by Tyagaraja (shown in MDIS composite in lower left), have a steeper UV-VIS slope than hollows like Sander, plotted in green (right MDIS image). Tyagaraja-type hollows also have a longer wavelength "inflection point," i.e., where the spectral ratio slope changes from positive to negative, than Sander-type hollows.

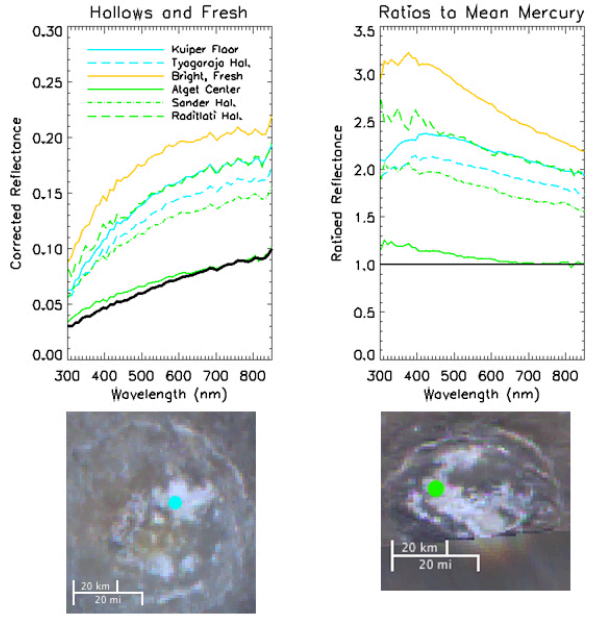

Fig. 3. Spectra of hollows and a small, very bright, fresh-looking crater. Hollows such as Tyagaraja (left) have stronger UV-VIS slope than those such as Sander (right).

UV through NIR characteristics are summarized in Fig. 4. All materials examined have steeper UV-VIS slopes (lower 310-nm/390-nm ratio) than mean Mercury. LRM is distinguished by lower reflectance in the visible, and LRM and pyroclastic materials have lower VIS/NIR ratio than mean Mercury. They also have lower UV-VIS slopes relative to hollows and fresh craters. The two hollows types appear to be distinguishable by UV features, with Tyagaraja-type (Hollows 1 in Fig.4) having steeper UV-VIS slopes.

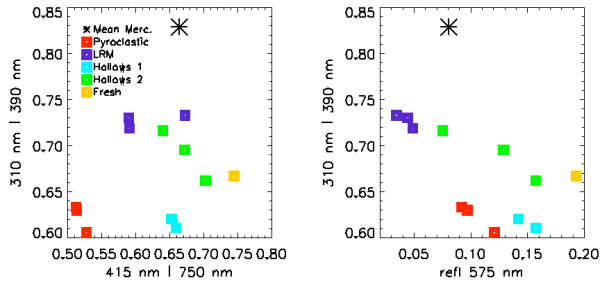

Fig. 4. All the units from Figs. 2 and 3 are combined in two spectral parameter comparison plots. Left is the VIS-NIR ratio vs. the VIS-UV ratio; right is visible reflectance vs. VIS-UV ratio. Star is mean Mercury.

UV Spectral Variations: UV absorptions may be indicative of oxygen-metal charge transfer (OMCT) absorptions in minerals [8], with metals such as Fe and Ti. OMCT absorptions are stronger than crystal-field absorptions and so may be seen in reflectance spectra when 1-μm absorptions are not. Given the abundance of Ti (<1wt% derived upper limit) and Fe (~4wt%), indicated by XRS measurements [9], Fe is more likely to be the main cause of an OMCT band on Mercury. Laboratory observations of low-Fe silicates [10-12] and glasses have shown that small weight percentages of iron result in spectra with an absorption having a strong UV-VIS slope from ~300 to 390 nm (Fig. 5).

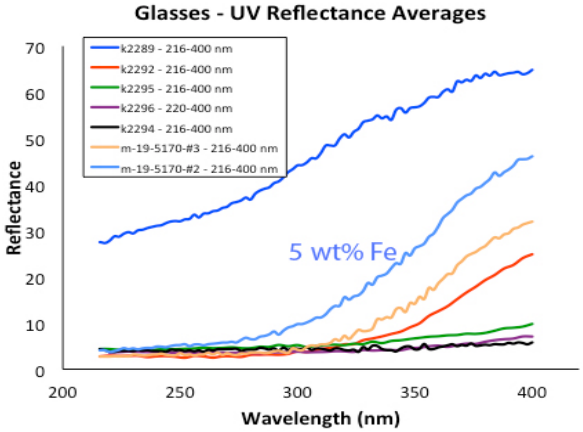

Fig. 5. Laboratory spectra of glass samples [12], from iron-free (dark blue) to 22 wt% Fe (purple and black). The UV-VIS slope of low-iron glasses, similar to those for low-iron pyroxenes [10,11], are consistent with VIRS spectra. Higher iron contents have less steep UV absorptions and overall lower reflectance.

Variation in iron content, consistent with XRS-derived values, may be responsible for some or much of the UV slope variations seen by MASCS. More laboratory measurements are needed to make a compelling link with Mercury spectra, however. If this link can be made, the lower UV-VIS slopes of LRM and pyroclastic materials may indicate relatively higher iron content than fresh craters or hollows, and the diversity in hollows types may imply different iron mineralogies in morphologically similar terrains. Currently, our laboratory measurements are limited to a maximum wavelength of ~400 nm, but systematic quantitative measurements of low-iron and low-titanium silicates and glasses through the NIR are underway [12] in an effort to determine if UV slope features can be diagnostic of iron content or mineralogy of Mercury materials.

Acknowledgements: NASA's Discovery Program and grants NNX10AI58G (PGG), NNX11AQ47G (PMDAP), and NNX11AO54G (LASER) supported this work.

References: [1] Solomon, S.C., et al. (2001) *Planet. Space Sci. 49*, 1445–1465. [2] McClintock, W.E., and Lankton, M.R., (2007) *Space Sci. Rev. 131*, 481–522. [3] McClintock, W.E., et al. (2008) *Science 321*, 62–65. [4] Hawkins, S. E., II, et al. (2007) *Space Sci. Rev. 131*, 247–338. [5] Denevi, B. W., et al. (2009) *Science 324*, 613–618. [6] Head, J. W., et al. (2008) *Science 321*, 69–72. [7] Blewett, D.T., et al. (2011) *Science 333*, 1856–1859. [8] Cloutis, E.A., et al. (2008), *Icarus 197*, 321. [9] Nittler, L.R., et al. (2011) *Science 333*, 1847–1850. [10] Klima, R.L., et al. (2007) *Meteorit. Planet. Sci. 42*, 235–253. [11] Klima, R.L., et al. (2011) *Meteorit. Planet. Sci. 46*, 379–395. [12] Greenspon, A.S., et al. (2012) *LPS 43*, this meeting.